https://dx.doi.org/10.1016/j.carbon.2021.10.023

Constructing resilient solid electrolyte interphases on carbon nanofiber film for advanced potassium metal anodes

*Rui Zhou, Hong Tan, Yao Gao, Zhen Hou, Xiaoqiong Du, and Biao Zhang**
Department of Applied Physics, The Hong Kong Polytechnic University, Hung Hom, Hong Kong, China.
*Corresponding author. Tel: (+852) 34003260. E-mail: biao.ap.zhang@polyu.edu.hk

Abstract

Stable cycling of potassium metal anodes in classic carbonate electrolytes remains a great challenge. Three-dimensional carbon hosts have been widely adopted to address the low Coulombic efficiency and devastated dendrite growth, but a correlation between the carbon microstructure and potassium plating/stripping stability is yet to be established. Here, stark contrasted carbonization temperatures, i.e., 800 and 2800 °C, are applied to electrospun carbon nanofiber (CNF) films for regulating graphitization degree. The resulted CNFs demonstrate distinct stability when serving as hosts for potassium metal anodes. We reveal that the carbon microstructure has a huge impact on not only the nucleation and diffusion of the K ions but also the mechanical properties of solid electrolyte interphases (SEIs). The maximum elastic deformation energy (U), which reveals the combined effects of Young's modulus and yield strain, is utilized to reflect the capability of SEI in accommodating the electrode deformation upon K deposition. The CNFs prepared at 2800 °C benefit the formation of a high U-value SEI. Consequently, it exhibits a small polarization and an ultra-long life of over 2000 h at 0.5 mA cm^{-2} in the carbonate electrolyte.

Keywords:
potassium metal anode, carbon host, solid electrolyte interphase, mechanical property

1. Introduction

The revival of potassium-ion batteries (PIBs) in recent years relies on both the natural abundance of potassium elements and the similarities between alkali metal-ion batteries.[1-3] The insertion chemistries of K ions resemble those of Li/Na ions to a large extent, which would greatly facilitate the quest for high-energy electrodes.[4, 5] For instance, several cathode candidates, such as $K_3V_2(PO_4)_2F_3$ and $K_xFeMnCN_6$, are inherited from the counterparts in Li- and Na-ion batteries.[6-8] The high content of potassium in the earth's crust brings about potential benefits in sustainability, making PIBs attractive candidates for large-scale energy storage. Among various anodes for PIBs, K metal has attracted intensive attention due to its high specific capacity (687 mAh g^{-1}) and low redox potential.[9-12] Notable improvement of PIBs is projected if the implementation of K metal anode is realized. The utilization of K metal anode will not only boost the performance of the anode but also enrich the development of the cathode.[13, 14] High-performance cathodes, including metal fluoride, sulfur, and oxygen electrode would be possible since K ions could be provided by the anode.[15-18]

K metal anode is afflicted primarily by the dendrite growth and low Coulombic efficiency. The formation of dendrite arises from the non-uniform plating-stripping process, which is widely observed in metal electrodes as a result of diffusion-limited growth.[12, 13, 19] Heterogeneous K ion flux originated from uneven local electric field distribution would further facilitate the formation of K dendrites, posing a risk to

short circuit.[19] Moreover, the K deposition on the anode brings about a large volume change, which may break the solid electrolyte interphase (SEI). The integrity of SEI is essential to maintain high Coulombic efficiency during K plating/stripping.[12, 20] Repeated fracture-formation of SEI would continuously consume the K ions and lead to a short lifetime.[21, 22] To overcome these obstacles, several constructive strategies have been reported, ranging from electrode design to electrolyte optimization.[14, 22-28] Carbon materials in various forms, such as graphene foam and carbon nanotube films, have been wildly adopted as host electrodes for accommodating K metal thanks to their high surface area and excellent conductivity.[29-31] For instance, a 10000-min (167 h) cycle time is achieved by David et al. through employing a rGO@3D Cu host in K metal batteries.[32] Along with the host design, regulating the SEI is also critical to realizing K metal anodes with long stability.[24, 33, 34] An exceptional Coulombic efficiency is obtained in Xiao et al.'s work, where a 1M KFSI/DME electrolyte is utilized. It reveals that the formation of a uniform and stable SEI is essential for achieving highly reversible K plating/stripping.[35]

Despite the above exciting achievements, stable K plating/stripping in carbonate electrolyte remains a great challenge. Carbonate electrolytes are commonly used in the Li-ion battery industry because of their wider electrochemical window, better temperature performance, and lower cost than ether-based counterparts. However, most of the previous works focus on the ether-based electrolytes with only a few reports on the carbonate ones,[23, 32, 36, 37] which generally show inferior performance. To achieve high-performance K metal anodes in carbonate electrolytes, it is essential to

simultaneously restrain the dendrite growth and construct a robust SEI. In this work, freestanding carbon nanofiber (CNF) matrixes are employed as hosts for K plating to mitigate the huge volume expansion/shrinkage. The surface functionality and microstructure of CNFs are tuned to increase the affinity between the K and CNFs. Furthermore, we demonstrate the carbon atomic structure greatly impacts the stability of SEI. The atomic force microscopy (AFM) shows a robust SEI is constructed on a CNF host that carbonized at 2800 °C. The SEI possesses a large maximum elastic deformation energy (U), offering the capability of accommodating the deformation during K growth. Consequently, stable cycling of K metal anode on CNF2800 is realized with decent Coulombic efficiencies.

2. Experimental section

2.1 Synthesis of CNFs and CNF@K electrodes

All chemicals used were of analytical grade. In a typical synthesis, 0.5 g polyacrylonitrile (PAN) was added in 10 mL of dimethylformamide (DMF), followed by magnetically stirring at 60 °C to obtain a homogenous solution. The electrospinning technique was then used to prepare nanofiber with a solution feeding speed of 1 mL h^{-1} and a voltage of 20 kV. The as-prepared nanofiber was pre-treated at 250 °C (heating rate of 2 °C min^{-1}) for 2 h in an air atmosphere for the oxidative stabilization of PAN, followed by a carbonization process at 800 °C (CNF800) and 2800 °C (CNF2800) under a flowing argon atmosphere.[38] CNF@K electrodes were prepared by immersing these CNFs into molten K.

2.2 Characterizations

The morphologies of CNFs were characterized by scanning electron microscopy (Field-emission SEM, TESCAN MAIA3 and transmission electron microscopy (TEM, JEOL 2010F). Raman scattering was carried out on a Witec-Confocal Raman system (UHTS 600 SMFC VIS) with an excitation wavelength of 532 nm. To investigate the chemical composition evolution of CNFs, Fourier transform infrared spectroscopy (FTIR) measurement was performed on a Bruker VERTEX 70 system. X-ray photoelectron spectrometry (XPS, Nexsa X-ray Photoelectron Spectrometer system) was employed to analyze the elemental composition of SEIs formed on different hosts. The microstructure of K growth on various hosts was examined by AFM using a Bruker Icon Dimension XR system under an Ar-filled glovebox.

2.3 Electrochemical measurements

CR2032 coin cells were assembled to evaluate the electrochemical performance. Cu foil or as-prepared CNFs were used as the working electrodes, with the counter electrode being a K metal plate. The separators consisted of glass fiber membrane (GF, Whatman) and PP (Celgard) with a structure of PP/GF/PP. 80 μL of 1M KFSI EC/DEC (provided by DoDo Chem. without further purification) was added as an electrolyte in each cell. Symmetric cells were also assembled with CNF@K electrodes or pure K metal electrodes. The electrochemistry impedance spectroscopy (EIS) was performed with a frequency range from 100 kHz to 10 mHz and voltage amplitude of 5 mV. Galvanostatic charge/discharge cycling was carried out on a land battery testing system (LAND CT2001A).

2.4 The mechanical test of SEI

Mechanical test was carried out in a glovebox using Bruker Dimension Icon AFM (Bruker, Santa Barbara, CA). An ACTA-20 (APPNANO) probe with a spring constant of 20 N m^{-1} was selected. A two-step nanoindentation test was conducted to determine Young's modulus (E) firstly under elastic deformation region and elastic strain limit (ε_Y) in the second step to intentionally break the SEI with a high force [39]. The maximum elastic deformation energy was calculated according to the following equation:

$$U=\frac{8}{15}\left(\frac{4}{5}\pi\right)^5 \cdot r^3 \cdot (1-\nu^2)^4 \cdot E \cdot (\varepsilon_Y)^5 \quad (1)$$

where ν is the SEI Poisson's ratio and r is radius of the rigid indenter (ν = 0.3, r = 1 μm).

3. Results and discussion

Both CNF800 and CNF2800 films exhibit porous network structures consisting of intertwined nanofibers, which could be used as freestanding electrodes (Figure 1a). The diameter of CNFs ranges from 100 to 300 nm. A sharp contrast in the nanostructure is observed in the TEM images, where CNF800 has an amorphous structure while clear graphitic domains presented in CNF2800 (Figure 1b, c and Figure S1, Supporting Information). FTIR is conducted to investigate the chemical composition of CNFs carbonized under different temperatures (Figure 1d). The absorption bands at around 1568, 1371, 1257, and 1192 cm^{-1} corresponding respectively to C=C absorption, C=N stretching vibration, C-N stretching, and C-C-C(O) are observed in CNF800, indicating the existence of oxygenated and nitrogenated functional groups, which are considered active towards K ions.[38] By contrast, these peaks disappear in CNF2800 due to the

elimination of heteroatoms under the high-temperature treatment. The degree of graphitization is characterized by Raman spectra (Figure 1e). There is a distinct 2D peak in the Raman spectra of CNFs annealed at 2800 °C compared to CNF800, attributing to an increased degree of graphitization. Nevertheless, there are still some defects or pores after carbonization at 2800 °C, as reflected by the prominent D band peak.[40, 41]

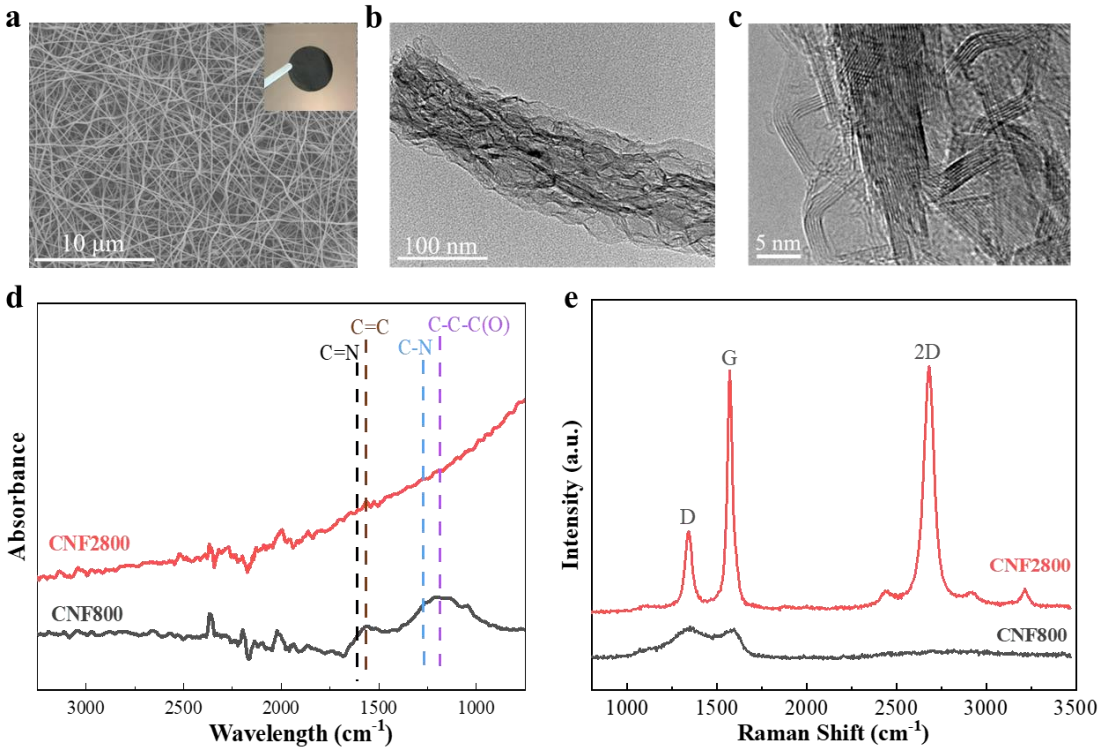

Figure 1. a) SEM image and b, c) TEM images of CNF2800. Inset in a) shows the optical image of a CNF freestanding electrode. d) FTIR spectra and e) Raman spectra of as-prepared CNFs.

Asymmetric cells are employed to evaluate the K plating and stripping behavior on Cu, as-prepared CNF800 and CNF2800 hosts, where K metal plates are used as counter/reference electrodes. The nucleation overpotential, which is defined as the

voltage difference between the voltage dip and platform of steady plating,[31, 42] is collected to assess K heterogeneous nucleation barrier on these samples. As shown in Figure 2a, sharp potential tip and large nucleation overpotential of 202 mV are observed on Cu, a reflection of the poor affinity between K and Cu, which would lead to non-uniform K deposition. On the contrary, CNF800 exhibits a much lower nucleation overpotential of 57 mV due possibly to the absorption of K ions to the carbon surface and defect sites as indicated by the monotonous decline in the initial discharge voltage profiles above 0 V.[38, 43] Similarly, a low nucleation overpotential of 42 mV is observed on CNF2800 during the discharge process. Before K plating, the K ions are intercalated into CNF2800 to form the graphite intercalation compound (GIC), as demonstrated by the blue shift of G band peak and the presence of a new peak at around 1610 cm^{-1} in the Raman spectra when discharged to 0 V (Figure S2, Supporting Information).[44-47] The results indicate the interactions between K and CNFs above 0 V improve the potassium affinity, leading to a smooth potential dip and small nucleation overpotential compared to that on the Cu electrode.

We further test the Coulombic efficiencies (CEs, the ratio of stripping to plating capacity during each cycle) at a current density of 1mA cm^{-2} with a deposition capacity of 1mAh cm^{-2} and a charge cutoff voltage of 1 V. As shown in Figure 2b, Cu exhibits relatively low CEs (below 80%) in the initial cycles which is attributed to the formation of SEI and consumption of electrolyte.[35] The CE of Cu increases to above 90% after 6 cycles but suffers from a sharp decrease from the 25^{th} cycle. The low Coulombic efficiency arises from two possible reasons: i) trapping of deposited K metal because

of the electric loss; and ii) SEI damage as a consequence of the severe dendrite growth and large volume expansion.[12, 48] In comparison, CNF800 exhibits a higher average CE of 93.4% but still suffers from degradation after 50 cycles. Notably, a stable and high average CE of 96% for 100 cycles is achieved on the CNF2800 matrix.

Similar enhancement is observed on the performance of symmetric cells where identical electrodes are employed as working and counter electrodes. Figure 2c shows the cyclic performance of cells cycled at a current density of 0.5 mA cm^{-2} with a capacity of 0.5 mAh cm^{-2}. The K|K battery has a large voltage hysteresis of ~0.6 V at the first cycle and gradually increases to ~0.77 V at 90 h. The cell is short circuit after 97 h due to the devastating dendrite growth, which eventually penetrates the separator. By contrast, the CNF800@K|CNF800@K maintains a stable overpotential of 0.5 V for 1500 h. After that, the voltage hysteresis begins to increase rapidly owing possibly to the unstable SEI. The CNF2800@K electrode delivers stable plating/stripping processes for over 2000 h with a relatively low hysteresis of 0.4 V owing to the high conductivity of CNF. The differences of K deposition on the three host electrodes become more obvious when cycling at a larger current density and higher capacity. The K|K cell fast shorts out at 33 h under 1 mA cm^{-2} with an areal capacity of 1 mAh cm^{-2} (Figure 2d), while the CNF800@K could stable charge/discharge for about 200 h. Surprisingly, the CNF2800@K|CNF2800@K cell still exhibits long-term stable cycling (800 h) with the lowest overpotential of ~0.55 V. Under increased current density and areal capacity, the CNF2800 still delivers a decent performance and remains the best among the three hosts (Fig. xx). Furthermore, the CNF2800@K also

delivers an excellent rate performance (Figure S3, Supporting Information). The voltage hysteresis of CNF2800@K|CNF2800@K symmetric cell are 0.3, 0.38, 0.48 and 0.74 V at a current density of 0.2, 0.5,1 and 2 mA cm^{-2}, respectively. In addition, when the current recovers to 0.2 mA cm^{-2}, the polarization also returns to its initial value. We also test the CNFs carbonized at a medium temperature of 1400 ^{o}C. As shown in Figure S4c and d, the cycling performance of CNF1400 is close to that of CNF2800 because of similar surface functionality. The nitrogenated and oxygenated groups have been removed at 1400 ^{o}C. Further increasing the temperature to 2800 ^{o}C improves the conductivity of CNFs [xx] for reducing the overpotential during K deposition. Therefore, we focus on CNF2800 to investigate the K plating behavior in partially graphitized carbon. Turning to the K|K cell, it shows much higher voltage hysteresis. What's worse, it exhibits violent vibration of voltage followed by a short-circuit failure when the current density is higher than 1 mA cm^{-2} due to the severe dendrite growth. A high current density would trigger severe dendrite growth due to the depletion of K ions on the electrode surface. The 3D CNF hosts with a large surface area essentially decrease the local current density and facilitate the charge transfer for obtaining a decent rate performance. Table S2 (Supporting Information) compares the electrochemical performance of CNF with that in the published work using carbonate electrolytes. The overall performance of CNF2800 is among the best considering the cyclic life and average Coulombic efficiency.

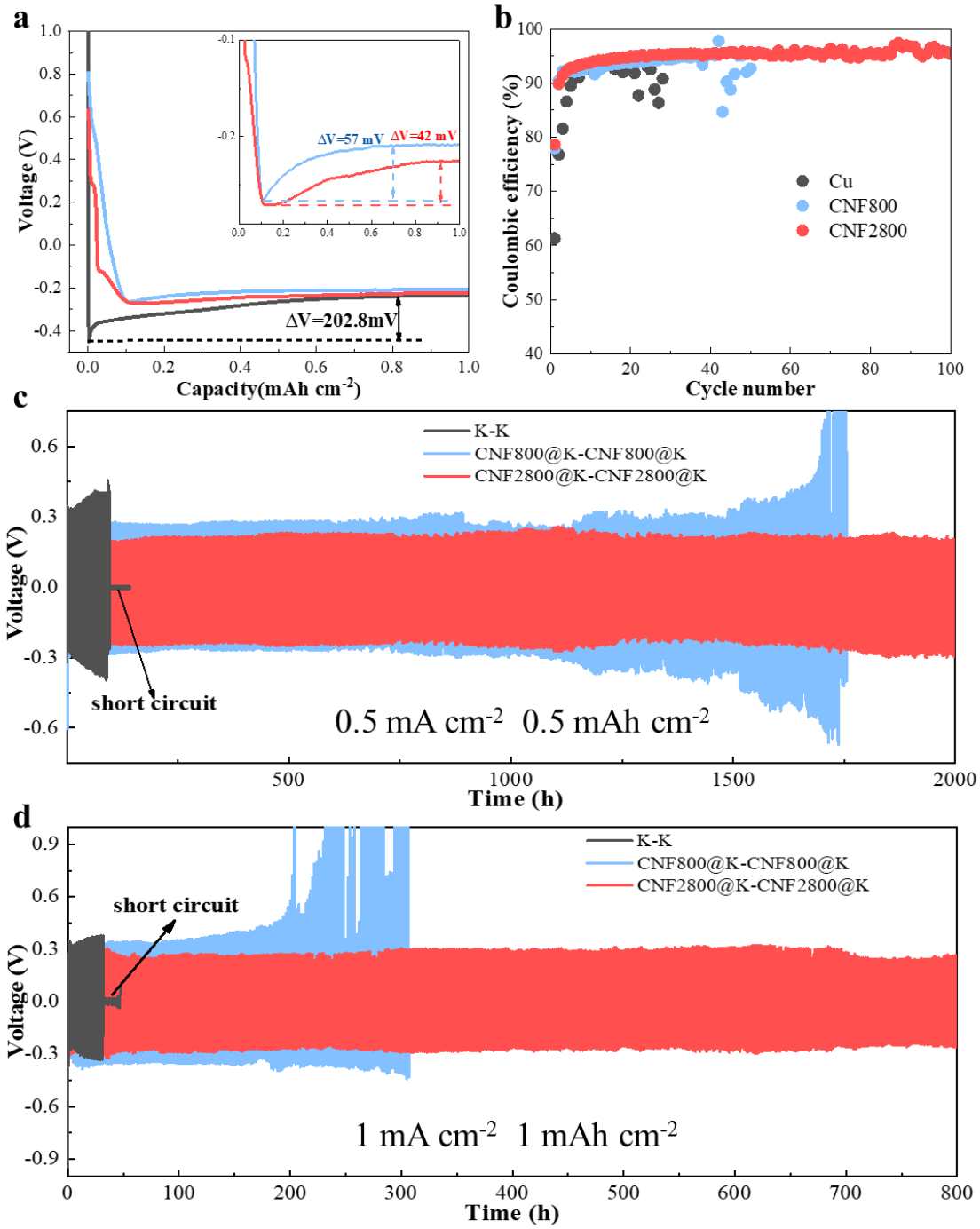

Figure 2. a) Voltage profiles of K plating on Cu, CNF800 and CNF2800 at a current density of 1mA cm^{-2}. b) The Coulombic efficiency of Cu, CNF800 and CNF2800 host at a current density of 1mA cm^{-2} with a capacity of 1 mAh cm^{-2}. Cycling performance of symmetric cells at c) 0.5 mA cm^{-2} with capacity of 0.5 mAh cm^{-2}, d) 1 mA cm^{-2} with capacity of 1 mAh cm^{-2}.

To explore the underlying mechanism for the improved electrochemical performance of CNF electrodes, the charge transfer behavior on the different hosts are investigated. As shown in Figure 3a, the K ion diffusion coefficients on Cu, CNF800 and CNF2800 are calculated according to the low-frequency region of EIS (Figure S4a, Supporting Information).[49] CNF2800 and CNF800 present a value of 3.2×10^{-21} cm^2 s^{-1} and 4.4×10^{-21} cm^2 s^{-1}, respectively, three orders of magnitude higher than that of Cu (8.8×10^{-24} cm^2 s^{-1}). The observation proves that CNFs provide fast diffusion channels for K ion, which is consistent with the much lower voltage hysteresis when using CNFs as hosts. Moreover, there is an increase of interfacial resistance (R_{CT}+R_{SEI}) for Cu foil after 10 cycles. In comparison, CNF2800 and CNF800 show lower resistance than Cu foil before cycling and deliver decreased interfacial resistance after 10 cycles, suggesting a gradual stabilization process. (Figure S4 and Table S1, Supporting Information).[32, 50]

Chronoamperometry (CA) tests are carried out to scrutinize further the K ion diffusion behavior and deposition mechanism on different hosts. The variation of current *versus* time at a constant voltage can reflect the change of the electrode surface morphology. Since the K metal deposition is under mass-transfer control, any increase in current during a potentiostatic electrodeposition can be assumed to be an increase in electrode surface area due to rugged K growth.[51-53] As shown in Figure 3b, a continuous increase of current density on Cu is observed when the voltage is maintained at -450 mv for 500 s, indicating a slow K ion diffusion and rough K deposition. Turning to CNF800 and CNF2800, the current densities keep steady at a lower value during the

whole deposition process, due to the stable K deposition behavior without increasing electrode surface area. The Sand's time is further investigated by depositing K on Cu and CNF matrixes at 2 mA cm^{-2} (Figure S5, Supporting Information), which is determined by the time when the apparent voltage divergence occurs because of complete ion depletion and accelerated dendrite growth.[31, 54] The voltage of Cu|K cell diverges after 3.6 h, whereas CNF800 and CNF2800 deliver Sand's time of 12 h and 16 h, respectively. The increased Sand's time of CNFs further confirms the improved K ion transports and the enhanced surface area, which reduce the local current density (Equation (S3), Supporting Information).

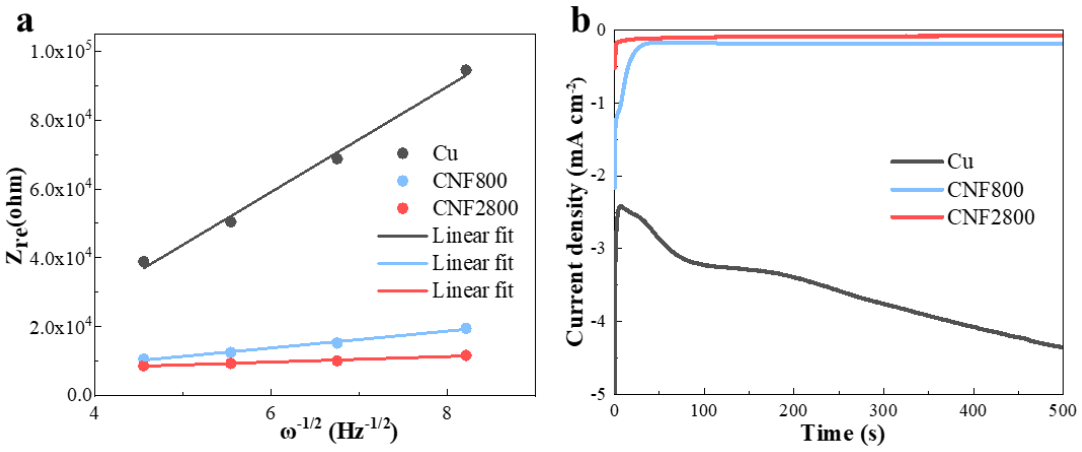

Figure 3. a) Corresponding curve of Z_{re} versus $\omega^{-1/2}$ (low-frequency regions) of Cu, CNF800 and CNF2800. b) Chronoamperograms (CAs) of Cu, CNF800 and CNF2800 half cells under a constant -450 mV overpotential.

The K metal deposition process on CNFs is examined under an Ar-filled glovebox using CNF2800 as the model material (Figure 4a-c). The pristine CNF2800 shows a typical fiber morphology with a smooth surface After plating K for 0.5 mAh cm^{-2}, the fibrous structure is retained but the surface become rough due to the growth of K metal

on the surface of the CNFs. Once the CNFs are fully covered, subsequent K metal starts to fill the voids among interlaced nanofibers. When the deposition capacity further increases to 1 mAh cm^{-2}, K metal begins to deposit on the top surface of the CNF electrode with a dendrite-free and flat morphology. The plating process of K on CNF800 is proved to be similar to that of CNF2800 (Figure S6, Supporting Information). The surface morphologies of the electrodes after plating of 1mAh cm^{-2} K metal are compared in Figure 4d-f. Mossy distribution of K particles with an uneven surface is observed on Cu foil and the surface roughness (Ra) is determined to be 188 nm, indicating a non-uniform K growth process. Such deposition tends to form dendrites and thus causes constant breakage and reconstruction of SEI during the K metal plating/stripping process, leading to relatively low CEs and fast end of cyclic life (Figure 2).[32] Conversely, K deposit on CNF matrixes exhibits smooth surface with much lower Ra values: 73.6 and 92.1 nm for CNF800 and CNF2800, respectively.

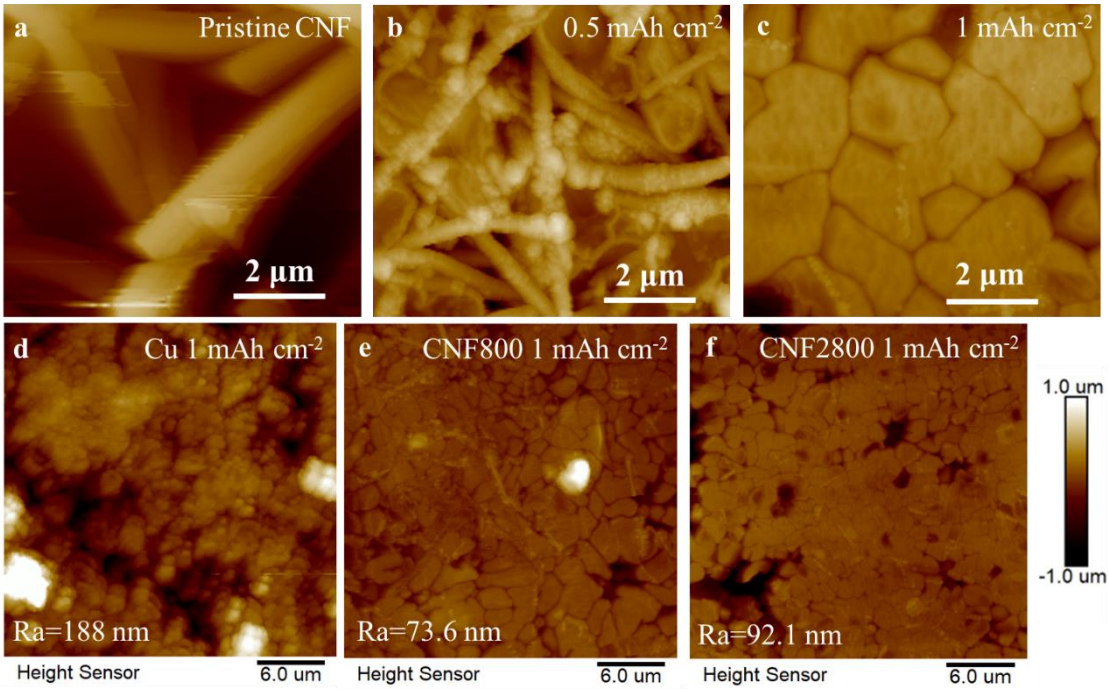

Figure 4. Morphology evolution of CNF2800: a) pristine one, b) after 0.5 mAh cm^{-2} K deposition and c) after1 mAh cm^{-2} K deposition; AFM images after deposition of 1 mAh cm^{-2} K on d) Cu foil, e) CNF800 and f) CNF2800.

The above analysis confirms the benefits of the 3D CNF host in guiding the K metal deposition for preventing non-uniform growth. Nonetheless, a question remains regarding the origin of the differences between CNF800 and CNF2800, which possess similar micro morphologies, comparable nucleation overpotentials, close K ion diffusion coefficients, analogous K deposition behavior and morphologies. It is widely accepted that the chemical composition and property of the SEI on carbon materials are affected by not only the electrolyte but also the chemical compositions and morphologies of carbon surfaces.[55-58] We speculate the microstructure of CNFs would significantly alter SEI properties. The resulted compositional differences of the SEI would bring about distinct mechanical stability upon deformation during K metal

plating. Therefore, the mechanical properties of SEI formed on different hosts are investigated by a two-step nanoindentation test based on AFM. The first test is conducted under a small loading to elastically deform the SEI, from where Young's modulus (E) is determined (Figure 5a). The elastic strain limit (ε_Y) is obtained in the second test, where a large force is applied to break the SEI intentionally (Figure 5b). For each sample, more than 70 test positions are conducted to calculate E and ε_Y for ensuring the reliability of the results. The maximum elastic deformation energy (U), which is proportional to the product of $E\cdot \varepsilon_Y^5$,[39] takes into account the combined effects of E and ε_Y and is adopted to reflect the capability of SEI in accommodating the deformation (Equation 1). As shown in Figure 5c, the SEI formed on Cu shows a much lower U value (37.83 pJ) than those in CNFs (87.93 pJ for CNF800 and 145.76 pJ for CNF2800), explaining the poor CE and cyclic performance to a certain extend. Surprisingly, the U value of SEI on CNF2800 is almost twice that of CNF800, accounting for the highly improved cycling performance of CNF2800 despite similar K deposition morphology.

The chemical compositions of SEI are analyzed to explore the reasons for the different U values. In general, the SEI could be treated as a nanocomposite where inorganic particles are distributed among the organic matrix. These inorganic particles assigned as K_2SO_3, K_2SO_4, $KHSO_4$, and KF in XPS, have much larger E than organic species. SEI formed on Cu possesses a high content of inorganic particles (Figure 5d), leading to a relatively large E value of 630 MPa but a poor elasticity of SEI (Figure 5a and b). The SEIs on the two CNFs show lower content of inorganic species, thus exhibit

lower E value than that of Cu (Figure 5a). Keeping in mind that both E and ε_Y play essential roles in determining the U-value of SEI. Thanks to the moderate content of inorganic components of SEI on CNF2800, it exhibits superior elasticity while keeping a reasonable modulus. We also investigate the SEI formed on CNFs without K metal plating by discharge to 0 V at a small current of 50 mA g^{-1}. It shows a similar trend where the SEI on CNF2800 has a slightly higher amount of inorganic components. It suggests that, apart from the electrolyte, carbon microstructure also has a significant impact on the SEI formation, which has also been observed in other electrode/electrolyte systems. Consequently, the largest value of U is obtained in CNF2800 for consuming the energy upon electrode swelling, leaving minor energy to break the SEI. Assisting by the high-U SEI, CNF2800 exhibits improved CE and long-term cyclic stability compared to CNF800.

The benefits of CNF2800 in boosting the K metal anode performance are illustrated in Fig. xx. Firstly, employing CNFs with abundant interconnected voids as 3D host enables massive loading of K and reduces the volume expansion during K plating. In addition, the as-prepared CNF scaffold efficiently reduces the effective local current density and facilitates K ion diffusion. As a result, it leads to a uniform K deposition and impedes the dendrite growth. Furthermore, the solid electrolyte interface (SEI) plays a crucial role in determining the cyclability of metal anodes. The SEI layers with different chemical compounds and mechanical properties are formed on CNF800 and CNF2800 due to their distinct structure and surface chemistry [1-3]. The SEI layer formed on CNF2800 has a high U value (reveals the combined roles of Young's

modulus and elastic strain limit), better accommodating the volumetric change. Owing to the synergistic effect between a 3D host and resilient SEI on CNF2800, highly improved coulombic efficiency and cycle life are achieved.

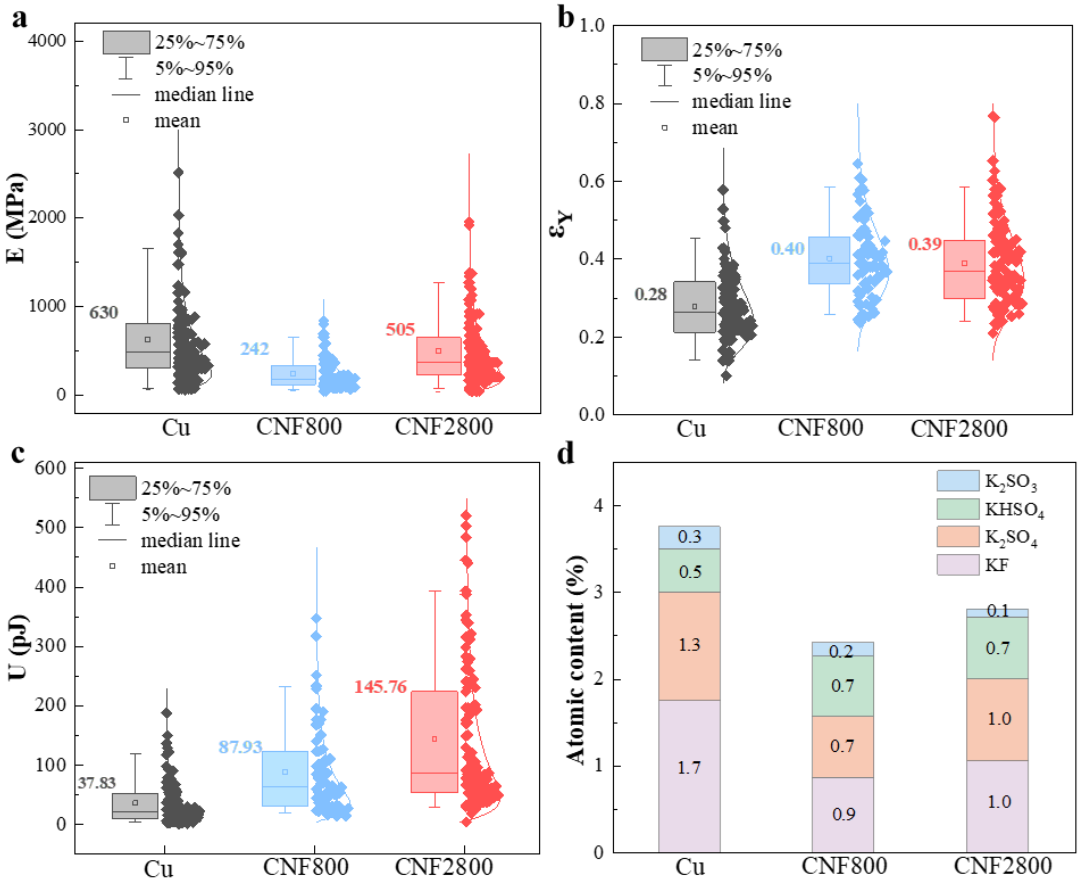

Figure 5. a) E, b) ε_Y and c) U value of the SEI layer formed on Cu, CNF800 and CNF2800 after 3 cycles. d) The atomic contents of inorganic particles in SEIs on Cu, CNF800 and CNF2800.

4. Conclusion

Carbon nanofibers with the distinct atomic structure are employed as hosts for stable K metal deposition. Owing to the reduced local current density, both CNFs exhibit improved plating/stripping behavior than Cu foil counterparts. The 3D CNFs facilitate the K ion diffusion, leading to a smooth morphology after K deposition. Although

having similar K metal nucleation and growth behavior, CNF2800 shows more attractive performance than CNF800 because of the formation of resilient SEI. The AFM test demonstrates that the SEI formed on CNF2800 has a large maximum elastic deformation energy (U) to consume the energy induced by anode expansion. Therefore, it holds a strong capability of accommodating the repeated swelling/contraction during K metal plating/stripping. Consequently, CNF2800 exhibits a high CE of 96% and stable long-term cycling for above 2000 h, which is among the most promising results for K metal anode in carbonate electrolytes. This work emphasizes the critical roles of carbon nanostructure in guiding the K metal deposition on the one hand. On the other hand, we demonstrate the surface functionality of carbon hosts significantly affect SEI's mechanical properties, which is largely ignored previously but of great importance to the long-term stability. We expect it would guide the rational design of carbon hosts for alkali metal anodes.

Acknowledgements
This work was supported by the General Research Fund (GRF) scheme of the Hong Kong Research Grants Council (15301220), the Hong Kong polytechnic University (ZVGH and ZVRP), and Guangdong-Hong Kong-Macau Joint Laboratory (2019B121205001).

References

[1] J.C. Pramudita, D. Sehrawat, D. Goonetilleke, N. Sharma, An review of the status of electrode materials for potassium-ion batteries, Adv. Energy Mater. 7(24) (2017) 1602911.

[2] W. Zhang, Y. Liu, Z. Guo, Approaching high-performance potassium-ion batteries via advanced design strategies and engineering, Sci. Adv. 5(5) (2019) eaav7412.

[3] J.D. Zhang, T.T. Liu, X. Cheng, M.T. Xia, R.T. Zheng, N. Peng, H.X. Yu, M. Shui, J. Shu, Development status and future prospect of non-aqueous potassium ion batteries for large scale energy storage, Nano Energy 60 (2019) 340-361.

[4] X. Ma, N. Xiao, J. Xiao, X. Song, H. Guo, Y. Wang, S. Zhao, Y. Zhong, J. Qiu, Nitrogen and phosphorus dual-doped porous carbons for high-rate potassium ion batteries, Carbon 179 (2021) 33-41.

[5] D. Wang, G. Du, D. Han, Q. Su, S. Ding, M. Zhang, W. Zhao, B. Xu, Porous flexible nitrogen-rich carbon membranes derived from chitosan as free-standing anodes for potassium-ion and sodium-ion batteries, Carbon 181 (2021) 1-8.

[6] R. Rajagopalan, Y. Tang, X. Ji, C. Jia, H. Wang, Advancements and challenges in potassium ion batteries: a comprehensive review, Adv. Funct. Mater. 30(12) (2020) 1909486.

[7] Q. Zhang, Z.J. Wang, S.L. Zhang, T.F. Zhou, J.F. Mao, Z.P. Guo, Cathode materials for potassium-ion batteries: current status and perspective, Electrochem. Energy Rev. 1(4) (2018) 625-658.

[8] X. Zhang, Z. Wei, K.N. Dinh, N. Chen, G. Chen, F. Du, Q. Yan, Layered oxide cathode for potassium-ion battery: recent progress and prospective, Small 16(38) (2020) 2002700.

[9] Y. Xu, C. Zhang, M. Zhou, Q. Fu, C. Zhao, M. Wu, Y. Lei, Highly nitrogen doped carbon nanofibers with superior rate capability and cyclability for potassium ion

batteries, Nat. Commun. 9(1) (2018) 1720.

[10] W. Wang, J.H. Zhou, Z.P. Wang, L.Y. Zhao, P.H. Li, Y. Yang, C. Yang, H.X. Huang, S.J. Guo, Short-Range Order in mesoporous carbon boosts potassium-ion battery performance, Adv. Energy Mater. 8(5) (2018) 1701648.

[11] H. Huang, J. Wang, X. Yang, R. Hu, J. Liu, L. Zhang, M. Zhu, Unveiling the advances of nanostructure design for alloy-type potassium-ion battery anodes via in situ TEM, Angew. Chemie. Int. Ed. 132(34) (2020) 14612-14618.

[12] W. Liu, P. Liu, D. Mitlin, Review of emerging concepts in SEI analysis and artificial SEI membranes for lithium, sodium, and potassium metal battery anodes, Adv. Energy Mater. 10(43) (2020) 2002297.

[13] C. Wei, Y. Tao, H. Fei, Y. An, Y. Tian, J. Feng, Y. Qian, Recent advances and perspectives in stable and dendrite-free potassium metal anodes, Energy Storage Mater. 30 (2020) 206-227.

[14] H. Wang, D. Yu, X. Wang, Z. Niu, M. Chen, L. Cheng, W. Zhou, L. Guo, Electrolyte chemistry enables simultaneous stabilization of potassium metal and alloying anode for potassium-ion batteries, Angew. Chemie. Int. Ed. 58(46) (2019) 16451-16455.

[15] J. Ding, H. Zhang, W. Fan, C. Zhong, W. Hu, D. Mitlin, Review of emerging potassium–sulfur batteries, Adv. Mater. 32(23) (2020) 1908007.

[16] W. Wang, Y. Wang, C.-H. Wang, Y.-W. Yang, Y.-C. Lu, In Situ probing of solid/liquid interfaces of potassium–oxygen batteries via ambient pressure X-ray photoelectron spectroscopy: New reaction pathways and root cause of battery

degradation, Energy Storage Mater. 36 (2021) 341-346.

[17] W. Yu, K.C. Lau, Y. Lei, R. Liu, L. Qin, W. Yang, B. Li, L.A. Curtiss, D. Zhai, F. Kang, Dendrite-free potassium–oxygen battery based on a liquid alloy anode, ACS Appl. Mater. Interfaces 9(37) (2017) 31871-31878.

[18] K. Hu, L. Qin, S. Zhang, J. Zheng, J. Sun, Y. Ito, Y. Wu, Building a reactive armor using S-doped graphene for protecting potassium metal anodes from oxygen crossover in K–O_2 batteries, ACS Energy Lett. 5(6) (2020) 1788-1793.

[19] J. Park, J. Lee, M.H. Alfaruqi, W.J. Kwak, J. Kim, J.Y. Hwang, Initial investigation and evaluation of potassium metal as an anode for rechargeable potassium batteries, J. Mater. Chem. A 8(33) (2020) 16718-16737.

[20] C.M. Efaw, B. Lu, Y. Lin, G.M. Pawar, P.R. Chinnam, M.F. Hurley, E.J. Dufek, Y.S. Meng, B. Li, A closed-host bi-layer dense/porous solid electrolyte interphase for enhanced lithium-metal anode stability, Mater. Today (2021) DOI: 10.1016/j.mattod.2021.04.018..

[21] Y. Gu, W.W. Wang, Y.J. Li, Q.H. Wu, S. Tang, J.W. Yan, M.S. Zheng, D.Y. Wu, C.H. Fan, W.Q. Hu, Z.B. Chen, Y. Fang, Q.H. Zhang, Q.F. Dong, B.W. Mao, Designable ultra-smooth ultra-thin solid-electrolyte interphases of three alkali metal anodes, Nat. Commun. 9(1) (2018) 1339.

[22] L. Xue, H. Gao, W. Zhou, S. Xin, K. Park, Y. Li, J.B. Goodenough, Liquid K–Na alloy anode enables dendrite-free potassium batteries, Adv. Mater. 28(43) (2016) 9608-9612.

[23] J. Wang, J. Yuan, C. Chen, L. Wang, Z. Zhai, Q. Fu, Y. Liu, L. Dong, W. Yan, A.

Li, J. Zhang, Cu_3Pt alloy-functionalized Cu mesh as current collector for dendritic-free anodes of potassium metal batteries, Nano Energy 75 (2020) 104914.

[24] J. Touja, P.N. Le Pham, N. Louvain, L. Monconduit, L. Stievano, Effect of the electrolyte on K-metal batteries, Chem. Commun. 56(93) (2020) 14673-14676.

[25] P. Hundekar, S. Basu, X. Fan, L. Li, A. Yoshimura, T. Gupta, V. Sarbada, A. Lakhnot, R. Jain, S. Narayanan, Y. Shi, C. Wang, N. Koratkar, In situ healing of dendrites in a potassium metal battery, Proc. Natl. Acad. Sci. U.S.A. 117(11) (2020) 5588-5594.

[26] M. Ye, J.-Y. Hwang, Y.-K. Sun, A 4 V class potassium metal battery with extremely low overpotential, ACS Nano 13(8) (2019) 9306-9314.

[27] N. Xiao, J. Zheng, G. Gourdin, L. Schkeryantz, Y. Wu, Anchoring an artificial protective layer to stabilize potassium metal anode in rechargeable $K–O_2$ batteries, ACS Appl. Mater. Interfaces 11(18) (2019) 16571-16577.

[28] P. Liu, Y. Wang, H. Hao, S. Basu, X. Feng, Y. Xu, J.A. Boscoboinik, J. Nanda, J. Watt, D. Mitlin, Stable potassium metal anodes with an all-aluminum current collector through improved electrolyte wetting, Adv. Mater. 32(49) (2020) 2002908.

[29] Y. Xie, J. Hu, Z. Han, H. Fan, J. Xu, Y. Lai, Z. Zhang, Ultra-stable K metal anode enabled by oxygen-rich carbon cloth, Nano Res. 13(11) (2020) 3137-3141.

[30] X. Zhao, F. Chen, J. Liu, M. Cheng, H. Su, J. Liu, Y. Xu, Enhanced surface binding energy regulates uniform potassium deposition for stable potassium metal anodes, J. Mater. Chem. A 8(11) (2020) 5671-5678.

[31] X. Tang, D. Zhou, P. Li, X. Guo, B. Sun, H. Liu, K. Yan, Y. Gogotsi, G. Wang,

MXene-based dendrite-free potassium metal batteries, Adv. Mater. 32(4) (2020) 1906739.

[32] P. Liu, Y. Wang, Q. Gu, J. Nanda, J. Watt, D. Mitlin, Dendrite-free potassium metal anodes in a carbonate electrolyte, Adv. Mater. 32(7) (2020) 1906735.

[33] W. Xu, H. Wang, J. Hu, H. Zhang, B. Zhang, F. Kang, D. Zhai, A highly concentrated electrolyte for high-efficiency potassium metal batteries, Chem. Commun. 57(8) (2021) 1034-1037.

[34] H.W. Wang, J.Y. Hu, J.H. Dong, K.C. Lau, L. Qin, Y. Lei, B.H. Li, D.Y. Zhai, Y.Y. Wu, F.Y. Kang, Artificial solid-electrolyte interphase enabled high-capacity and stable cycling potassium metal batteries, Adv. Energy Mater. 9(43) (2019) 1902697.

[35] N. Xiao, W.D. McCulloch, Y. Wu, Reversible dendrite-free potassium plating and stripping electrochemistry for potassium secondary batteries, J. Am. Chem. Soc. 139(28) (2017) 9475-9478.

[36] P.C. Shi, S.P. Zhang, G.X. Lu, L.F. Wang, Y. Jiang, F.F. Liu, Y. Yao, H. Yang, M.Z. Ma, S.F. Ye, X.Y. Tao, Y.Z. Feng, X.J. Wu, X.H. Rui, Y. Yu, Red phosphorous-derived protective layers with high ionic conductivity and mechanical strength on dendrite-free sodium and potassium metal anodes, Adv. Energy Mater. 11(5) (2021) 2003381.

[37] Y. Li, L. Zhang, S. Liu, X. Wang, D. Xie, X. Xia, C. Gu, J. Tu, Original growth mechanism for ultra-stable dendrite-free potassium metal electrode, Nano Energy 62 (2019) 367-375.

[38] X. Lin, J. Huang, B. Zhang, Correlation between the microstructure of carbon materials and their potassium ion storage performance, Carbon 143 (2019) 138-146.

[39] Y. Gao, X. Du, Z. Hou, X. Shen, Y.-W. Mai, J.-M. Tarascon, B. Zhang, Unraveling the mechanical origin of stable solid electrolyte interphase, Joule (2021) DOI: https://doi.org/10.1016/j.joule.2021.05.015..

[40] B. Zhang, C.M. Ghimbeu, C. Laberty, C. Vix-Guterl, J.M. Tarascon, correlation between microstructure and Na storage behavior in hard carbon, Adv. Energy Mater. 6(1) (2016) 1501588.

[41] A.C. Ferrari, J.C. Meyer, V. Scardaci, C. Casiraghi, M. Lazzeri, F. Mauri, S. Piscanec, D. Jiang, K.S. Novoselov, S. Roth, A.K. Geim, Raman spectrum of graphene and graphene layers, Phys. Rev. Lett. 97(18) (2006) 187401.

[42] Z. Hou, Y. Yu, W. Wang, X. Zhao, Q. Di, Q. Chen, W. Chen, Y. Liu, Z. Quan, Lithiophilic Ag nanoparticle layer on Cu current collector toward stable Li metal anode, ACS Appl. Mater. Interfaces 11(8) (2019) 8148-8154.

[43] J. Yang, Z. Ju, Y. Jiang, Z. Xing, B. Xi, J. Feng, S. Xiong, Enhanced capacity and rate capability of nitrogen/oxygen dual-doped hard carbon in capacitive potassium-ion storage, Adv. Mater. 30(4) (2018) 1700104.

[44] K. Share, A.P. Cohn, R.E. Carter, C.L. Pint, Mechanism of potassium ion intercalation staging in few layered graphene from in situ Raman spectroscopy, Nanoscale 8(36) (2016) 16435-16439.

[45] J.C. Chacón-Torres, L. Wirtz, T. Pichler, Manifestation of charged and strained graphene layers in the Raman response of graphite intercalation compounds, ACS Nano 7(10) (2013) 9249-9259.

[46] P. Shi, T. Li, R. Zhang, X. Shen, X.B. Cheng, R. Xu, J.Q. Huang, X.R. Chen, H.

Liu, Q. Zhang, Lithiophilic LiC_6 layers on carbon hosts enabling stable Li metal anode in working batteries, Adv. Mater. 31(8) (2019) 1807131.

[47] Q. Zhao, X. Hao, S. Su, J. Ma, Y. Hu, Y. Liu, F. Kang, Y.-B. He, Expanded-graphite embedded in lithium metal as dendrite-free anode of lithium metal batteries, J. Mater. Chem. A 7(26) (2019) 15871-15879.

[48] T. Mukra, E. Peled, Elucidation of the losses in cycling lithium-metal anodes in carbonate-based electrolytes, J. Electrochem. Soc. 167(10) (2020) 100520.

[49] Z. Hou, W. Wang, Q. Chen, Y. Yu, X. Zhao, M. Tang, Y. Zheng, Z. Quan, Hybrid protective layer for stable sodium metal anodes at high utilization, ACS Appl. Mater. Interfaces 11(41) (2019) 37693-37700.

[50] K. Lin, X. Qin, M. Liu, X. Xu, G. Liang, J. Wu, F. Kang, G. Chen, B. Li, Ultrafine titanium nitride sheath decorated carbon nanofiber network enabling stable lithium metal anodes, Adv. Funct. Mater. 29(46) (2019) 1903229.

[51] Z. Zhao, J. Zhao, Z. Hu, J. Li, J. Li, Y. Zhang, C. Wang, G. Cui, Long-life and deeply rechargeable aqueous Zn anodes enabled by a multifunctional brightener-inspired interphase, Energy Environ. Sci. 12(6) (2019) 1938-1949.

[52] C.J. Lan, C.Y. Lee, T.S. Chin, Tetra-alkyl ammonium hydroxides as inhibitors of Zn dendrite in Zn-based secondary batteries, Electrochim. Acta 52(17) (2007) 5407-5416.

[53] R.Y. Wang, D.W. Kirk, G.X. Zhang, Effects of deposition conditions on the morphology of zinc deposits from alkaline zincate solutions, J. Electrochem. Soc. 153(5) (2006) C357.

[54] L. Qin, Y. Lei, H.W. Wang, J.H. Dong, Y.Y. Wu, D.Y. Zhai, F.Y. Kang, Y. Tao, Q.H. Yang, Capillary e of metallic potassium in aligned carbon nanotubes for use as stable potassium metal anodes, Adv. Energy Mater. 9(29) (2019) 1901427.

[55] P.B. Balbuena, Y.X. Wang, Lithium-ion batteries: solid-electrolyte interphase, World Scientific 2004.

[56] S.J. An, J. Li, C. Daniel, D. Mohanty, S. Nagpure, D.L. Wood, The state of understanding of the lithium-ion-battery graphite solid electrolyte interphase (SEI) and its relationship to formation cycling, Carbon 105 (2016) 52-76.

[57] P. Peljo, H.H. Girault, Electrochemical potential window of battery electrolytes: the HOMO–LUMO misconception, Energy Environ. Sci. 11(9) (2018) 2306-2309.

[58] N. Mubarak, F. Rehman, J. Wu, M. Ihsan-Ul-Haq, Y. Li, Y. Zhao, X. Shen, Z. Luo, B. Huang, J.-K. Kim, Morphology, chemistry, performance trident: Insights from hollow, mesoporous carbon nanofibers for dendrite-free sodium metal batteries, Nano Energy 86 (2021) 106132.